EUROPEAN FUSION DEVELOPMENT AGREEMENT

EFDA–JET–PR(07)10

M. Ariola, D. Mazon, D. Moreau, F. Piccolo, F. Sartori, G. De Tommasi,
L. Zabeo and JET EFDA contributors

Integrated Plasma Shape and Boundary Flux Control on JET Tokamak

Integrated Plasma Shape and Boundary Flux Control on JET Tokamak

M. Ariola[1], D. Mazon[3], D. Moreau[3], F. Piccolo[4], F. Sartori[4], G. De Tommasi[2], L. Zabeo[4] and JET EFDA contributors*

[1]Associazione EURATOM-ENEA-CREATE, Universitµa di Napoli Parthenope, via Medina 40, 80133 Napoli, Italy
[2]Associazione EURATOM-ENEA-CREATE, Universitµa di Napoli \Federico II", via Claudio 21, 80125, Napoli, Italy
[3]EURATOM-CEA Association, DSM-DRFC, Cadarache, 13108, St. Paul lez Durance, France
[4]EURATOM-UKAEA Fusion Association, Culham Science Centre, Abingdon, OX14 3DB, UK
** See annex of M.L. Watkins et al, "Overview of JET Results ", (Proc.□21st IAEA Fusion Energy Conference, Chengdu, China (2006)).*

Preprint of Paper to be submitted for publication in
Fusion Science and Technology

ABSTRACT

Advance tokamak (AT) scenarios are gaining more and more importance in operating tokamaks. These scenarios pose challenging control problems, since they require the simultaneous achievement of ambitious plasma parameters. The inherent coupling among the various variables calls for an integrated approach for the design of the controllers. This paper describes an example of integrated design recently implemented at JET: the control of plasma shape and boundary flux. After a brief description of the control problem, the paper focuses on the solution that has been adopted, presenting the technical details of the control scheme. The experimental results included in the paper are in agreement with the expected simulation results, and demonstrate the effectiveness of the proposed solution.

1. INTRODUCTION

Recently, many experiments in operating tokamaks and, as a consequence, a lot of effort in the research on tokamak control, have focused on the so-called advanced tokamak scenarios (AT, [1{3]). An advanced tokamak plasma can be defined as a plasma where the following conditions are simultaneously obtained: stationary state; a high plasma kinetic pressure; a large fraction of self-driven current; a sufficiently good particle and energy confinement. AT scenarios are aimed at allowing steady-state operation without the need to drive a large amount of plasma current by external non-inductive drive systems, thus making them more efficient.

In the AT scenarios, in order to achieve these simultaneously challenging plasma performance, several control problems need to be adequately resolved. Amongst these problems, shape control plays an essential role: first of all accurate control is needed to obtain the plasma shapes required to achieve high β values [33]; these shapes need to be precisely controlled for a number of reasons such as optimization of the coupling with the additional heating systems, avoidance of wall interactions, divertor shape optimization for pumping. This task is complicated by the fact that the "extreme" shapes typically pursued in AT scenarios are characterized by a large elongation, which makes even the vertical stabilization difficult to guarantee in the presence of unexpected large disturbances, such as for instance like Edge-Localised Modes (ELMs). Moreover in order to achieve and maintain extreme shapes, the feedback controller needs to regulate many different points all around the plasma boundary.

Another key ingredient to improve the energy confinement and to increase the non-inductive current fraction in AT regimes is the active control of the internal pressure and current profiles. Since the external current drive sources usually are not sufficient to reach the desired values of non-inductive current, the *bootstrap* current [4, 5] should be maximized. One way to increase the boostrap fraction is to generate an Internal Transport Barrier (ITB, [6, 7]). In presence of an ITB there is a reduction of turbulence transport and therefore an increase of confinement. The plasma pressure profile shows a strong internal gradient which produces a bootstrap current peak at the location of the maximum gradient. Some real-time experiments to control the strength of the ITB [8] clearly

demonstrated the necessity of controlling at the same time the current density profile. Indeed the link between ITB triggering and the current density profile is something which is now well known.

In the most sophisticated control schemes presently adopted on tokamaks [9, 10], the current profile control is obtained using feedback controllers that make use of the additional heating devices available on the machine. The inherent, unavoidable coupling among the feedback loops, calls for a cautious design of the various controllers: whereas some feed-back controllers can be designed neglecting the presence of other loops, more typically the controllers interfere with each other. In these cases, when the controlled and the control variables cannot be tightly separated, the best approach is the integrated design of the various controllers. This approach implies that when a certain feedback loops is tuned, it must take into account all the other loops that can interact with it.

This paper presents an example of integration between two control loops performed at JET: the plasma shape control and the boundary °flux control. Most present tokamaks operate inductively with current control; steady-state discharges should in principle be fully noninductive. These discharges call for new operational methods that maintain constant zero loop voltage at the plasma boundary, as has been demonstrated at Tore Supra [11] and DIII-D [12]. Therefore obtaining effective and routine boundary °flux control is an essential step in AT regime. For this reason, at JET an integrated approach for the control of the plasma shape and boundary °flux has been developed, implemented and tested on a high triangularity ITER-relevant plasma [13].

The paper is divided as follows. In Section II, after a brief introduction on the poloidal field coils system, the JET Shape Controller (SC) is described [14], focusing on its structure and its different control modes. Special attention is then given to the new *eXtreme Shape Controller* (XSC), which is now available at JET, and whose architecture has been used to implement the plasma boundary flux control loop. Section III describes the way the boundary flux controller has been designed. Finally Section IV presents the experimental results recently obtained at JET.

2. THE JET TOKAMAK

This section gives an overview of the *Joint European Torus* (JET) experiment, as well as a description of the plasma shape control system. A full description of the JET tokamak can be found in [15], and some experimental results recently achieved on that machine are reported in [16, 17]. A technical description of JET systems can be found in [18]. More details about plasma current, position and shape control at JET can be found in [19], while the XSC algorithm is fully described in [20].

The JET tokamak has been constructed in the late seventies and early eighties with the aim of defining the parameters, the size and the working conditions of a tokamak reactor. This was to include the study of alpha-heating, which implies a reasonable *amplification factor Q*, which is defined as the ratio of the fusion power to the externally applied heating power. In 1997, 16 MW of fusion power have been generated by a heating power of 26 MW, corresponding to $Q \cong 0.6$ [21]. This result has been achieved using a *deuterium-tritium* plasma. Good results have been obtained using deuterium plasmas as well.

Today the JET continues to make a valuable contribution in preparation for the future high *Q* operation of ITER [13] through the development of plasma scenarios and by addressing key physics and technical issues.

A. THE POLOIDAL FIELD COILS SYSTEM

In a tokamak machine, the poloidal field (PF) coils are the actuators available to control the plasma current, position and shape. Figure 1 shows a poloidal cross-section of the JET tokamak where the PF coils are shown as red squares. These coils are linked together into 10 circuits driven by independent power supplies, named *P1*, *P4*, *IMB*, *SHA*, *PFX*, *D1*, *D2*, *D3*, *D4* and *FRFA*.

The *P1* circuit enables both the plasma inductive formation and the control of the plasma current. *FRFA* is used to stabilize the plasma vertical unstable mode by means of a feedback loop, while the other eight circuits are used to shape and move the plasma column within the toroidal chamber.

The current in the *FRFA* circuit is driven by the *Vertical Stabilization Controller* [22]. The remaining PF circuits are controlled either by the SC or by the XSC to perform both plasma current and shape control, as it is described in the next sections.

B. THE JET SHAPE CONTROLLER

The SC drives the current into the PF circuits, and it was conceived as the solution to the shape control problem for the entire discharge.

During the plasma formation process, the SC controls the currents in PF circuits so that they track a set of pre-programmed waveforms. These waveforms have been empirically shown to give a successful breakdown. Afterwards a small plasma column is formed and slowly expands to ¯ll the vessel volume. In this phase, since it is difficult to calculate the plasma shape precisely, the SC controls only the plasma current and the radial position. Depending on the experiment, different aspects of the shape become more important. The main experimental phase typically starts after the plasma becomes bounded by a separatrix, and the control is switched to the *geometrical descriptors* which specify the plasma boundary (gaps, strike points and X-point position shown in Figure 2).

The SC gives the possibility of controlling simultaneously up to six geometrical descriptors. This limitation has been overcome by the XSC which has been deployed at JET in 2003: as explained later, with this new system it is possible to control, in a mean-square sense, more than 30 plasma shape descriptors using eight PF circuits. The person responsible for implementing an experiment (the *Session Leader*) programs the discharge dividing it in a number of *time windows*; in each time window, the PF circuits can be used in one of the following control modes:

CURRENT CONTROL the controlled variable is the current in the corresponding circuit; this is the case for instance of the breakdown phase;
PLASMA CURRENT CONTROL the controlled variable is the plasma current;
GAP CONTROL the controlled variable is a plasma boundary geometrical descriptor, typically a gap;

BLOCKED the current in the actuator is set to 0;
FREE-WHEELING the voltage across the coil is set to 0.
The definition of the variables that can be selected in *gap control* mode, as well as the availability of the different control modes, differs for each PF circuit. For example the *plasma current control* mode is available only for the *P1* circuit.

The SC design is based on a plasma linear model; only one model is used for all the cases of interest. The SC designers managed to obtain a controller that guarantees acceptable dynamic performance [23] in many different situations. This result has been achieved limiting the control bandwidth and tuning the controller parameters during the SC commissioning phase. The Session Leader is able to obtain the desired plasma configuration choosing different control variables in different time windows of the experiment.

The SC design is based on the model of the PF coils system, which can be written as

$$\begin{aligned} \mathrm{V}_{PF}(t) = & \begin{bmatrix} L_1 & M_{12} & \cdots & M_{1N} \\ M_{12} & L_2 & \cdots & M_{2N} \\ \vdots & \vdots & \ddots & \vdots \\ M_{1N} & M_{2N} & \cdots & L_N \end{bmatrix} \mathrm{I}_{PF}(t) + \begin{bmatrix} L_1 & \cdots & M_{12} & \cdots & M_{1N} \\ M_{12} & \cdots & L_2 & \cdots & M_{2N} \\ \vdots & & \vdots & \ddots & \vdots \\ M_{1N} & \cdots & M_{2N} & \cdots & L_N \end{bmatrix} \mathrm{I}_{PF}(t) \\ = & \mathrm{M}\mathrm{I}_{PF}(t) + \mathrm{R}\mathrm{I}_{PF}(t), \end{aligned} \tag{1}$$

which is valid in the absence of plasma. The terms L_i represents the self-inductance of the i-th circuit, while M_{ij} is a mutual inductance term. $\mathbf{V}_{PF}(t)$ is the vector of power supply output voltages, $\mathbf{I}_{PF}(t)$ is the vector of measured currents in the PF coils, and R_i are the circuit resistances.

The control algorithm implemented by the SC, which is independent of the choice of control modes, is given by

$$\mathbf{V}_{ref}(\mathrm{t}) = \hat{\mathbf{R}}\mathbf{I}_{PF}(\mathrm{t}) + \mathbf{K}\,(\mathbf{Y}_{ref}(t) - (t)) \tag{2}$$

In (2), $\mathbf{V}_{ref}(t)$ are the voltage references to the amplifiers; **R** is an estimation of matrix **R** in (1); **K** is the gain matrix; $\mathbf{Y}_{ref}(t)$ and $\mathbf{Y}(t)$ are the reference signals and measurements, respectively, and depend on the controlled variables choice. A schematic of the SC is shown in Figure 3.

The control matrix K is constructed according to

$$\mathbf{K} = \hat{\mathbf{M}}\mathbf{T}^{-1}\,\mathbf{\Lambda} \tag{3}$$

where $\hat{\mathbf{M}}$ is an estimation of the mutual inductance matrix in (1) and decouples the PF circuits, $\mathbf{\Lambda}^{-1}$ is the diagonal matrix of desired time constants, and **T** is the transformation matrix, which represents the linearized relation between the currents in the PF circuits and the measurements

$$\mathbf{Y}(t) = \mathbf{T}\mathbf{I}_{PF}(t) \tag{4}$$

Replacing relation (4) into (1), the open-loop system model reads

$$\mathbf{M}\mathbf{T}^{-1}\,\dot{\mathbf{Y}}(t) = \mathrm{V}_{PF}(t) - \mathbf{R}\mathbf{I}_{PF}(t). \tag{5}$$

Using equations (2)–(5), the closed-loop system can be written as

$$\mathbf{Y}(t) = \mathbf{\Lambda}(\mathbf{Y}ref(t) - \mathbf{Y}(t). \tag{6}$$

The model in (6) is derived neglecting the delays introduced by the power supplies and by the diagnostics, and assuming $\hat{\mathbf{R}} = \mathbf{R}$ and $\mathbf{M} = \hat{\mathbf{M}}$.

It follows that for all the PF circuits set in *current control* mode, the corresponding Y(t) entries are the PF currents, and the corresponding block in the matrix T is the identity matrix.

After the plasma is formed, the plasma current circuit should be added in (1). The SC adopts a simplified model of the plasma current circuit, where the plasma resistance is neglected, and only the mutual inductance with the *P1* circuit is retained. Since the plasma current distribution is a function of the magnetic fields, the mutual induction between *P1* and the plasma depends on the currents in the circuits. However, this dependence is not relevant, and the following broadly valid linear model can be derived

$$\dot{I}p(t) = -c\;\dot{I}_{P1}(t)\text{ , with } c > 0. \tag{7}$$

where $I_p(t)$ and $I_{P1}(t)$ are the plasma current and the current in the *P1* circuit, respectively. Model (7) is over-simplified since it does not take into account any plasma internal profile concise parameters, such as, for instance, beta poloidal β_p and the internal inductance l_i [24].

The model (7) is then used to determine the row corresponding to the plasma current in the T matrix, when *P1* is set in *plasma current control* mode.

C. THE EXTREME SHAPE CONTROLLER

1. Control algorithm

The XSC controls the whole plasma shape, specified as a set of geometrical descriptors (typically 32), calculating the PF coil current references. Its design [20] is based on the following plasma linearized state space model [25, 26], which relates the variations of the PF currents to the variations of the geometrical descriptors around a given equilibrium:

$$\delta\boldsymbol{x}(t) = \mathbf{A}\delta\mathbf{x}(t) + \mathbf{B}\delta\mathbf{u}(t), \tag{8}$$

$$I_{peq}\delta\mathbf{g}(t) = \mathbf{C}\;\delta\mathbf{I}_{PF}(t), \tag{9}$$

where:

- **A**, **B** and **C** are the model matrices;

- $\delta \boldsymbol{x}(t) = [\delta \mathbf{I}^{\mathrm{T}}_{PF}(t)\ \delta I_p(t)]^{\mathrm{T}} \in \mathbb{R}^{(nPF+1)}$ is the state space vector, which includes the currents in the $n_{PF}(= 8)$ PF circuits available for the plasma shape control, and the plasma current I_p;
- $\delta \mathbf{u}(t) = [\delta \mathrm{V}^{\mathrm{T}}_{PF}(t)\ 0]^{\mathrm{T}} \in \mathbb{R}^{(nPF+1)}$ is the input voltages vector;
- $\delta \mathbf{g}(t)\ 2\ \mathrm{R}nG$ are the $n_G(\leq 32)$ shape descriptors variations;
- I_{peq} is the equilibrium value of the plasma current.

Let $\mathbf{I}_{PFN}(t)$ be the PF currents normalized to the equilibrium plasma current, it follows that

$$\delta \mathrm{g}(t) = \mathbf{C}\ \delta \mathrm{I}_{PFN}(t). \tag{10}$$

The model (8)-(9) is obtained neglecting the effects of the plasma profile parameters $\delta\beta_p(t)$ and $\delta l_i(t)$, which can be regarded as disturbances.

From (10) it also follows that the plasma boundary descriptors have the same dynamic response of the PF currents. The shape controller design has been based on the C matrix.

Since $n_{PF} < n_G$, in principle it is possible to control to zero the error on n_{PF} linear combinations of geometrical descriptors. It was chosen to minimize the following steady-state performance index:

$$J = \lim_{t \longrightarrow +\infty} (\delta \mathrm{g}_{ref} - \delta \mathrm{g}(t))^T (\delta \mathrm{g}_{ref} - \delta \mathrm{g}(t)) \tag{11}$$

where $\delta \mathbf{g}_{ref}$ are *constant* references to the geometrical descriptors.

Minimization of (11) can be attained using the Singular Value Decomposition (SVD) of the **C** matrix:

$$\mathbf{C} = \mathbf{U}\,\mathbf{S}\,\mathbf{V}^{\mathrm{T}},$$

where the matrix S contains the singular values, U and V are unitary matrices, that is

$$\mathbf{U}\,\mathbf{U}^{\mathrm{T}} = \mathbf{U}^{\mathrm{T}}\mathbf{U} = \mathbf{I}\ ,\ \mathbf{V}\,\mathbf{V}^{\mathrm{T}} = \mathbf{V}^{\mathrm{T}}\mathbf{V} = \mathbf{I},$$

As a matter of fact, using the JET linearized models, it turned out that some singular values (typically 2 or 3, depending on the configuration) are one order of magnitude smaller than the others. This fact implies that minimizing the performance index (11) retaining all the singular values result in a high control effort at steady-state, in terms of PF coil currents. For this reason, the XSC achieves a trade-off condition, minimizing a modified quadratic cost function that penalizes both the error on the controlled shape descriptors, and the control effort. This is achieved controlling to zero the error only for the $\bar{n} < n_{PF}$ linear combination related to the largest 5 or 6 singular values [27].

A more sophisticated version of the XSC has then been implemented introducing weight matrices both for the geometrical descriptors and for the PF coil currents. The reason for this lies in the fact

that there are some regions of the plasma boundary where more tight requirements are requested, for instance for the antenna power coupling. Also, the PF coil currents available for feedback purposes differ significantly from coil to coil and among different scenarios. As a consequence, the determination of the controller gains is based on the SVD of the following weighted model output matrix:

$$\tilde{\mathbf{C}} = \tilde{\mathbf{Q}}\mathbf{C}\,\tilde{\mathbf{R}}^{-1} \tag{12}$$

where $\tilde{\mathbf{Q}}$ and $\tilde{\mathbf{R}}$ are two diagonal matrices used to weight the errors on the controlled outputs and the currents into the PF coils, respectively.

The control scheme has been implemented using $\bar{n}$ proportional-integral (PI) regulators.

2. Control Architecture

The XSC has been designed to operate on the JET tokamak; thus special efforts have been made to minimize the impact on the existing control systems. For this reason the XSC uses the SC to control the currents into the PF coils.

Figure 4 shows the XSC architecture. Here the *current controller* block is the SC in which the *P1* circuit is set in *plasma current control* mode and the remaining eight PF circuits are set in *current control* mode. This block performs both plasma current control and the decoupling of the PF coils circuits: each PF circuit can be treated as an independent SISO (*single-input-single-output*) channel with a first order response.

The low-pass filters in Figure 4 set the time constants for all the PF circuits to the slowest one τ_{PF}. Therefore the *i*-th PF circuit can be modeled as:

$$I_{PFi}(s) = \frac{1}{1 + sT_{PF}}\, I_{PF_{ref_i}}(s)\,,$$

where $I_{PFi}(s)$ and $I_{PFrefi}(s)$ are the Laplace transforms of the *i*-th PF current measurements and reference, respectively.

The *gap controller* block shown in Figure 4 computes the $\bar{n}$ linear combinations of the geometrical descriptors that are controlled to zero at steady-state. Then these $\bar{n}$ controlled quantities are projected onto the PF currents space.

The structure of the *gap controller* is depicted in Figure 5, where the matrices $\mathbf{V}_M$, $\mathbf{S}_M$ and $\mathbf{U}^T_M$ corresponds to the $\bar{n}$ largest singular values of the SVD in (12), and where eight PI's are used instead of the needed $\bar{n}$. With this architectural choice, it is possible to exploit the anti wind-up system of the integral actions to constraint the PF currents between the operational limits. Note that the PI's are the same for all the channels.

3. BOUNDARY FLUX CONTROL

This section deals with the design of the boundary flux controller for the JET tokamak, and it

also describes how this controller has been implemented using the XSC architecture presented in II C. This solution enables the simultaneous control of the entire plasma shap and of the magnetic boundary flux.

The actuator that has been chosen to control the plasma boundary flux ψ_b is the current in the *P1* circuit. Indeed an analysis of the influence of the currents on the boundary flux has shown that the other circuits are much less efficient and therefore it is much worth to use them for the shape control.

As has been shown in the previous section, the standard configuration of the XSC makes use of eight PF circuits to control the plasma shape, while the control of the *P1* circuit is left to the SC for the plasma current regulation. When controlling ψ_b, the SC releases the control of the *P1* current to the XSC, setting this circuit to *current control* mode. A new actuator is then available to the XSC and it is used to control ψ_b, with negligible influence on the shape. Note that when the XSC controls ψ_b the plasma current is not feedback controlled, and it is left floating between given bounds.

The first step for the design of the boundary flux controller is the determination of a dynamic model that relates the boundary flux ψ_b to the current in the *P1* circuit.

To determine such a model, both ψ_b and *IP1* are added to the linear model (8)–(9).

It follows that, for the boundary °flux control, 9 PF coil are used, and the model output equation is given by 24

$$\varepsilon_{\%}(\mathrm{t}) = 100 \left| \frac{b_{ref}(t) - \ _b(t)}{b_{ref}(t)} \right|$$

For the boundary flux controller design, it is necessary to have a Single-Input-Single-Output (SISO) model in the form

$$\delta\psi_b(s) = W(s)\delta I_{P1}(s), \tag{13}$$

with the transfer function $W(s)$ of order as low as possible, to make the design easier. To arrive to a model in the form (13), the ¯first step is to consider the loop consisting of the XSC and the plant model (see the scheme in Figure 4). Then a model order reduction is needed so that a low-order model is obtained. In this case, a balanced model reduction [28] has been performed, arriving to a model of the fourth order.

Basing on model (13), a PI controller has been designed using the root-locus technique [29]. The controller performance have been assessed by means of simulations carried out using the plasma full-order model; these simulations have shown that trying to improve the performance of the boundary flux controller using higher gains in the PI controller induces dangerous oscillations on the PF coil current. For this reason, a compromise solution has been adopted.

The boundary flux controller has been implemented within the XSC architecture shownin

Figure 4. When the ψ_b control is switched on, the *Ip* control is removed from the *current controller* block, and all the PF circuits, including *P1*, are set to *current control* mode. To compute the *IP1* reference another channel is added to the *gap controller*, which is modified as shown in Figure 6. Note that the the PI controller on the *P1* channel (PI_1^*) is different from the ones on the shape controller channel, and it is the one tuned on the model (13). When the XSC is controlling the flux, the plasma current is left °floating between safe prescribed bounds; if it exceeds these bounds, a smooth termination of the pulse (*soft-stop*) is triggered [34].

Eventually the reference to the plasma boundary flux controller can be generated using one of the two systems shown in Figure 7:

RTMX system which generates *Ãbref* either with a real-time waveform generator or as the output of another real-time control system;

Session Leader Interface which allows to generates ramp references with possibly different slopes in each time window.

4. EXPERIMENTAL RESULTS

The plasma boundary flux controller has been developed at JET in 2006 and it has been used during the 2006 experimental campaigns. Some of the results achieved during these campaigns are presented in this section.

The pulses described hereafter have been carried out with a toroidal magnetic field B_T = 3T, a nominal plasma current I_p = 1.5 MA, while the available additional heating powers during the 10s plasma current at-top was about 15 MW. The heating powers time traces are shown in Figure 8 for the JET Pulse No: 67840. During the *preheating* phase, which is defined as the time interval between the plasma formation and the main heating phase, only the LHCD actuator is used. Indeed during the *preheating* high performance plasmas can be obtained with a moderate heating power, achieving the desired target current density profile [30]. At the end of this section a brief discussion about how the plasma boundary flux control can be effectively used during this phase to improve performance will be given.

The target plasma shape used for the boundary flux control experiments presented in this section is shown in Figure 9. This shape is a modified version of the one developed for the ITER-relevant scenarios [31], which allows to reach high plasma density values, an early formation of a single-null X-point configuration, and the use of non-inductive current drive to tailor the current profile.

The experimental values of both plasma boundary flux $\psi_b(t)$ and current $I_p(t)$ for JET Pulse No: 67834 are shown in Figure 10(a). Here the reference is chosen as a ramp with a constant slope corresponding to a plasma loop voltage $V_l \cong$ = 95 mV.

The relative error between the plasma boundary flux reference and measurement is shown in Figure 10(b); it becomes smaller than 0.5% after 2s, which is the settling time of the control system. It is worth noting that, the dynamic performance of the boundary flux control is bottlenecked by the bandwidth of the *P1* power amplifier.

Keeping the slope of the boundary flux constant, since the additional heating powers are also constant during the control phase, the plasma current reaches a constant value of I_p = 1.4MA.

The boundary flux control has been also used to perform plasma loop voltage modulations, as it is shown in Figure 11. In this case the slope of $\psi_{bref}(t)$ is varied so as to obtain different values of V_l and I_p. Note that during this experiment the plasma current was left floating between 1:1 MA and 2.1 MA. Exceeding one of these limits would cause a termination of the pulse.

Figure 12 reports the plasma shape descriptors during the V_l modulation experiment. Although the plasma current acts as a disturbance for the shape control, the error on the shape is kept small. It is worth to notice that, since the XSC controls the plasma boundary over more than 30 shape descriptors in a mean-square sense, the error between measurements and references is always different from zero.

In the pulses reported in Figures 10 and 11, the boundary flux control starts during the plasma current *flat-top* phase, when the plasma current has already reached the target value. In the JET Pulse No: 68854 (see Figure 13) the boundary flux control has been switched on during the plasma current *ramp-up* phase, and the reference is such that I_p = 1.6 MA is obtained.

The ramp-up phase correspond to the *preheating* phase, thus it is very important because it preforms the target current density profile, which is crucial for improving the plasma performance. Future works at JET will be devoted to the integration of plasma shape (including boundary flux) with plasma current profile control [32]. Indeed controlling the boundary flux ψ_b enables to control indirectly the plasma current I_p via the edge value of the current density profile. The combination of distributed plasma current density profile and I_p control gives more °flexibility in the quest for performance and steady state discharges.

CONCLUSIONS AND FUTURE WORKS

In this paper we have presented an integrated approach for the simultaneous control of plasma shape and boundary flux, recently implemented at JET. This control scheme has been successfully tested during several experiments on high triangularity ITER-relevant plasmas; different reference on the boundary flux have been chosen, either with constant slope or slowly time-varying. This integrated control has been tested both during the plasma current flat-top phase and during the ramp-up phase.

At JET, in the near future, this controller will be integrated in a more general scheme with the objective of obtaining a centralized controller for the plasma shape, boundary flux, current and pressure profiles.

ACKNOWLEDGEMENTS

The authors would like to thank the JET Operator team, the session leaders Dr. Jerzy Brzozoswki and Dr. Isabel Nunes, the leader of the *XSC Phase II Enhancement Project* Dr. Flavio Crisanti, and the members of the CREATE team: Prof. Raffaele Albanese, Prof. Giuseppe Ambrosino, Prof. Massimiliano Mattei, Prof. Alfredo Pironti and Prof. Fabio Villone.

REFERENCES

[1]. T.S. Taylor, Plasma Physics and Controlled Fusion **39**, B47 (1997).

[2]. C. Gormezano, Plasma Physics and Controlled Fusion **41**, B367 (1999).

[3]. X. Litaudon, Plasma Physics and Controlled Fusion **47**, A1 (2006).

[4]. A.A. Galeev and R.Z. Sagdev, Soviet Physics - JETP **26,** 233 (1968).

[5]. R.J. Bickerton, J.W. Connor, and J. Taylor, Nature Physical Science **229**, 110 (1971).

[6]. R.C. Wolf, Plasma Physics and Controlled Fusion **45**, R1 (2003).

[7]. J. W. Connor et al., Nuclear Fusion **44**, R1 (2004).

[8]. D. Mazon et al., Plasma Physics and Controlled Fusion **44**, 1087 (2002).

[9]. D. Moreau et al., in *Proceedings of the* 20*th IAEA Fusion Energy Conference* (Vilamoura, Portugal, 2004).

[10]. L. Laborde et al., Plasma Physics and Controlled Fusion **47**, 155 (2005).

[11]. T. Wijnands, D. Van Houtte, G. Martin, X. Litaudon, and P. Froissard, Nuclear Fusion **37**, 777 (1997).

[12]. C.C. Petty et al., Nuclear Fusion **35**, 773 (1995).

[13]. M. Shimada, V. Mukhovatov, G. Federici, Y. Gribov, et al., Nuclear Fusion **44**, 350 (2004).

[14]. M. Garibba, R. Litunovsky, P. Noll, and S. Puppin, in *Proceedings of the* 15th *SOFE Conference* (1996), pp. 33-36.

[15]. J. Wesson, *The science of JET* (JET Joint Undertaking, Abingdon, Oxon, 2000), JET-R(99)13.

[16]. J. Pamela, E. R. Solano, and JET EFDA Contributors, Nuclear Fusion **43**, 1540 (2003).

[17]. M. L. Watkins on behalf of JET-EFDA contributors, in *Proceedings of* 21*st IAEA Fusion Energy Conference* (Chengdu, People's Republic of China, 2006).

[18]. Fusion Technology **11** (1987), special issue.

[19]. F. Sartori, G. De Tommasi, and F. Piccolo, IEEE Control Systems Magazine **26**, 64 (2006).

[20]. M. Ariola and A. Pironti, IEEE Control Systems Magazine **25**, 65 (2005).

[21]. M. Keilhacker, A. Gibson, C. Gormezano, P. Lomas, et al., Nuclear Fusion **39**, 209 (1999).

[22]. M. Lennholm, D. Campbell, F. Milani, F. Puppin, et al., in *Proceedings of the* 17th *SOFE Conference* (1997), vol. 1, pp. 539-542.

[23]. M. Garibba, M.L. Browne, D.J. Campbell, Z. Hudson, et al., Fusion Technology **1**, 747 (1994).

[24]. G. Ambrosino and R. Albanese, IEEE Control Systems Magazine **26**, 76 (2005).

[25]. R. Albanese and F. Villone, Nuclear Fusion **38**, 723 (1998).

[26]. R. Albanese, G. Calabrμo, M. Mattei, and F. Villone, Fusion Engineering and Design **66-68**, 715 (2003).

[27]. G. Ambrosino, M. Ariola, and A. Pironti, in 42nd *IEEE Conference on Decision and Control* (Maui, Hawaii, 2003), pp. 869-873.

[28]. K. Zhou and J. C. Doyle, *Essentials of Robust Control* (Prentice-Hall, Englewood Cliffs, NJ, 1998).

[29]. G. Franklin, J.D. Powell, and A. Emami-Naeini, *Feedback Control of Dynamic Systems* (Prentice-Hall, Englewood Cliffs, NJ, 2006), 5th ed.

[30]. T. Tala et al., Plasma Physics and Controlled Fusion **44**, 1181 (2002).
[31]. F.G. Rimini et al., Nuclear Fusion **45**, 1481 (2005).
[32]. D. Moreau et al., in *Proceedings of* 21*st IAEA Fusion Energy Conference* (Chengdu, People's Republic of China, 2006).
[33]. β is the ratio of plasma pressure to the magnetic field pressure, and it is one of the figure of merit for magnetic confinement.
[34]. When a soft stop is triggered, the additional heating system are turned off and the the plasma current is brought to zero following a prescribed waveform.

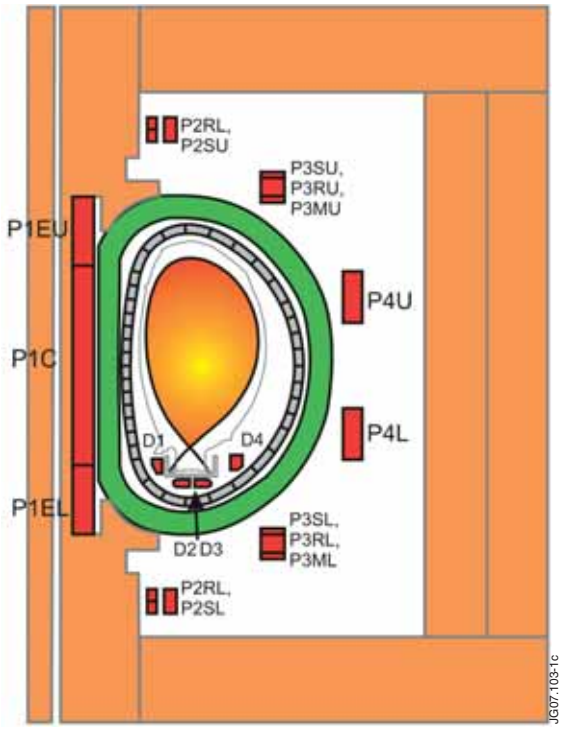

Figure1: The JET poloidal field coils system. The P1 *circuit includes the elements of the central solenoid P1EU, P1C, P1EL, as well as P3MU and P3ML. The series circuit of P4U and P4L is named* P4, *while the circuit that creates an imbalance current between the two coils is referred to as* IMB. SHA *is made of the series circuit of P2SU, P3SU, P2SL, and P3SL. The fast radial field circuit, termed* FRFA, *connects the P2RU, P3RU, P2RL, and P3RL. The central part of the central solenoid contains an additional circuit named* PFX, *which is used for plasma shape control.Finally the four divertor coils (*D1 *to* D4*) are driven separately each by one power supply.*

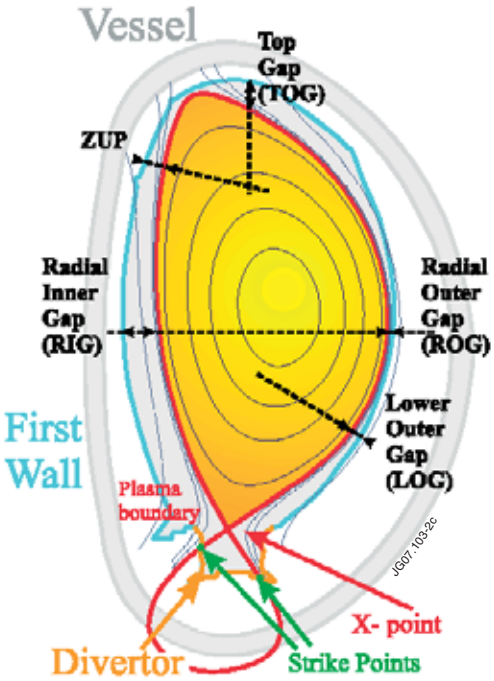

Figure 2: Plasma shape descriptors at JET. Note that a gap is not strictly the distance between the plasma surface and a point on the wall, but rather the distance measured on a fixed line. This definition simplifies the calculation and provides a good linear relationship between the currents in the PF coils and the geometrical descriptors. Even if the XSC can control up to 32 gaps, for clarity only few are shown in this figure.

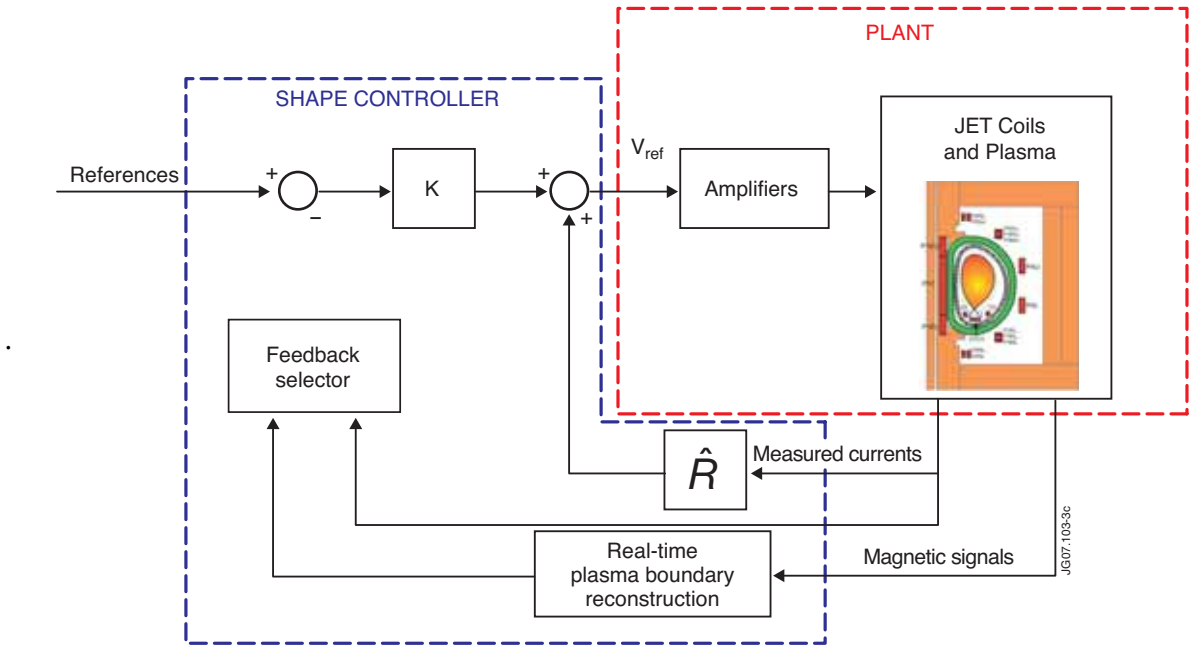

Figure3: Block diagram of the JET shape controller. The feedback selector allows to change among the available control modes

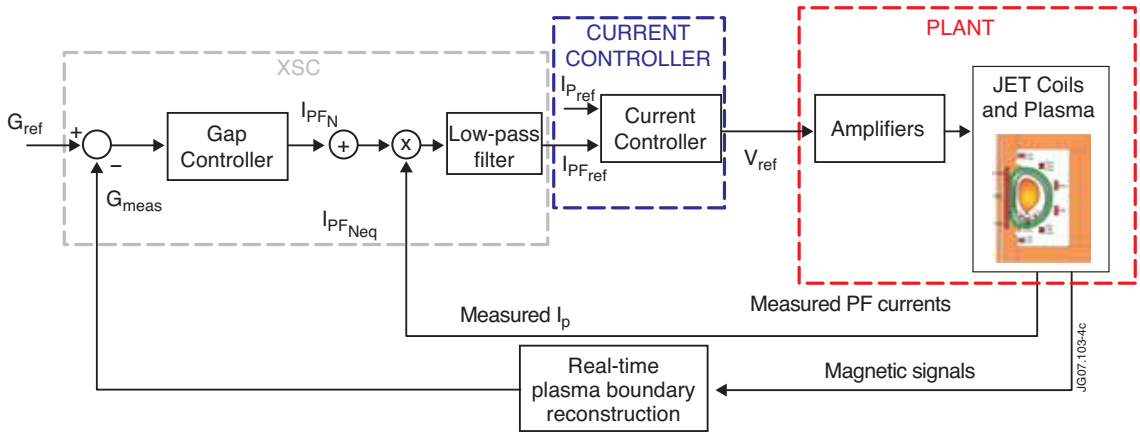

Figure 4: Block diagram of the eXtreme Shape Controller.

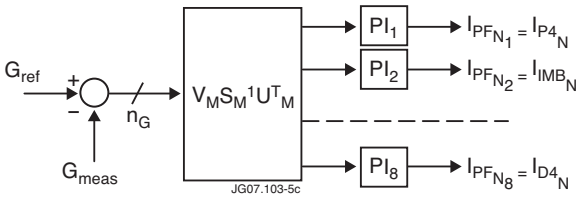

Figure 5: The XSC gap controller block.

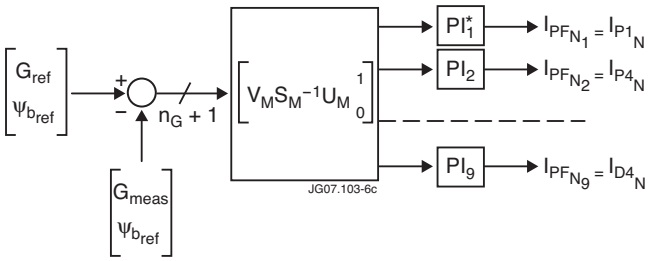

Figure 6: The modified gap controller block for plasma boundary flux control

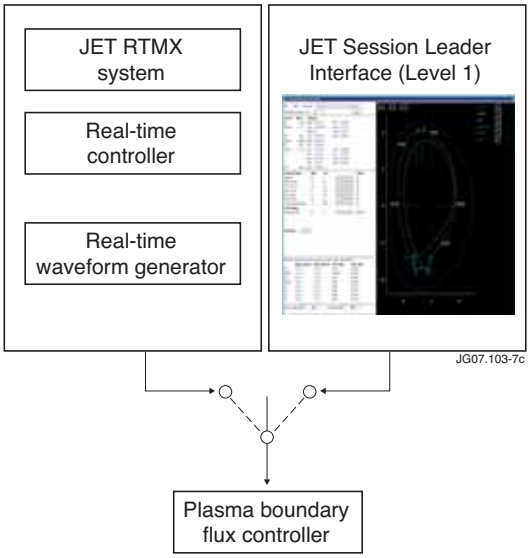

Figure 7: Systems interconnections.

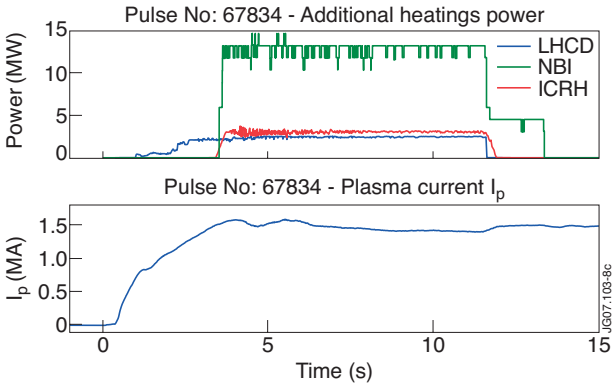

Figure 8: Additional heatings powers and plasma current of the JET Pulse No: 67834.

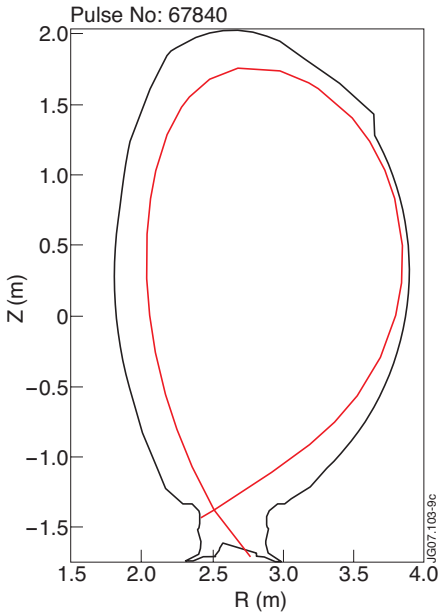

Figure 9: Plasma shape of the JET Pulse No: 67840. This shape has been used for the first boundary flux control experiments at JET.

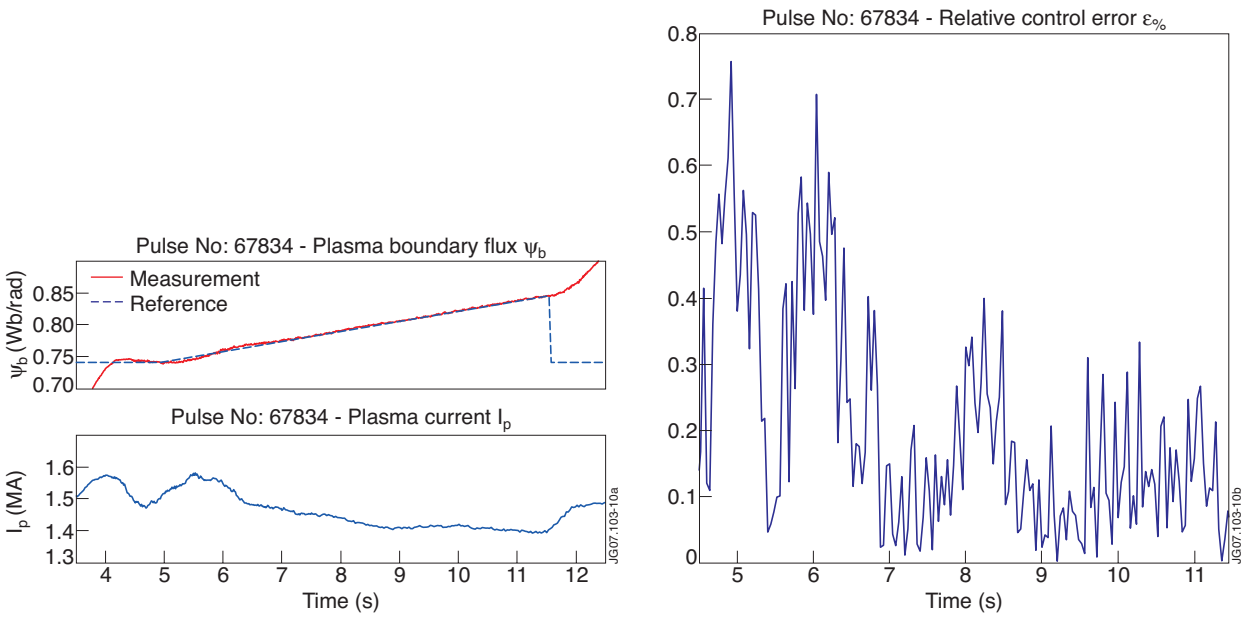

Figure 10: JET Pulse No: 67834 - plasma boundary flux control between t = 4.5s and t = 11.5s, with a constant slope ramp reference.

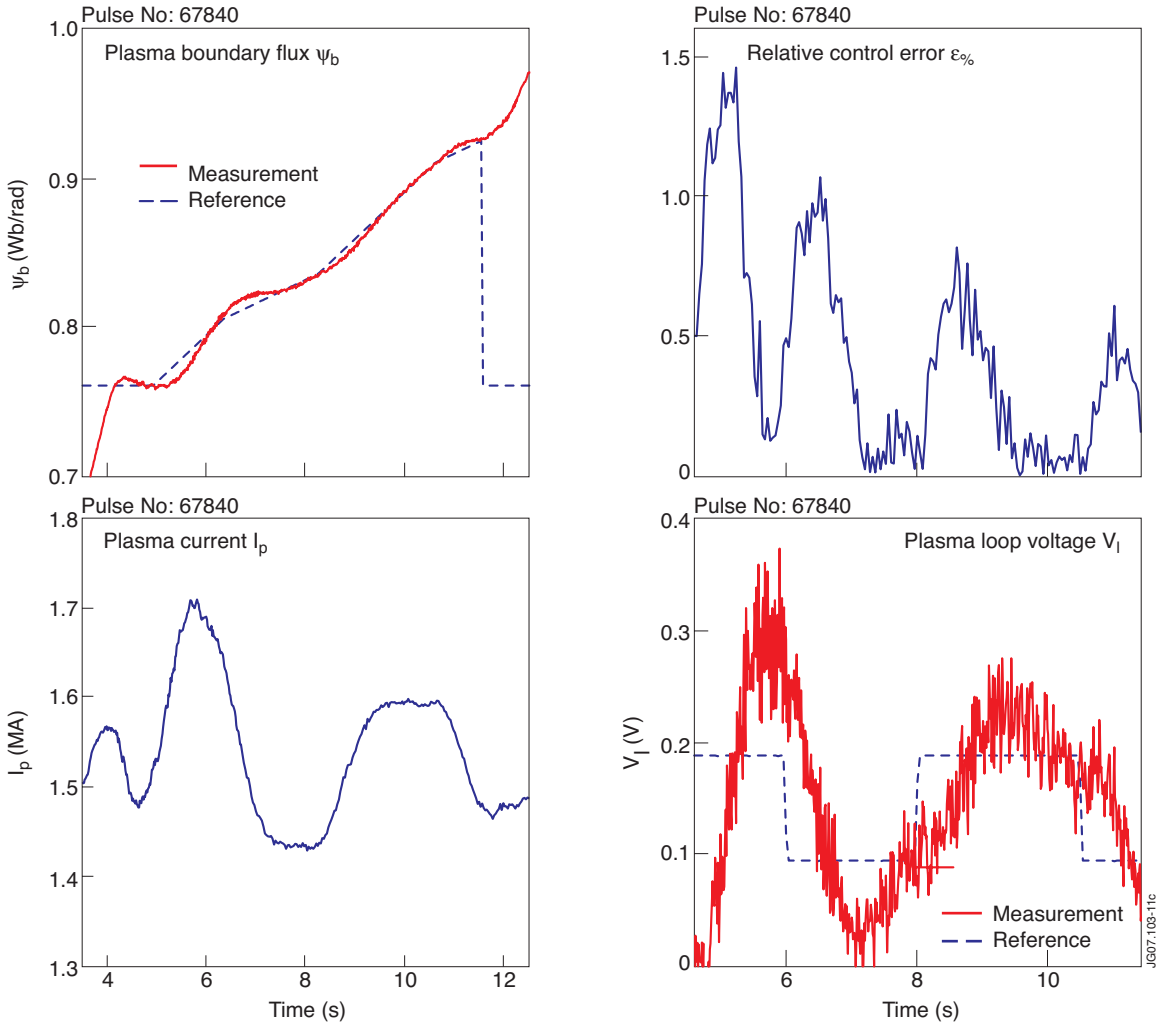

Figure 11: JET Pulse No: 67840 - boundary flux control is active between t = 4.5s and t = 11.5s, with a variable reference.

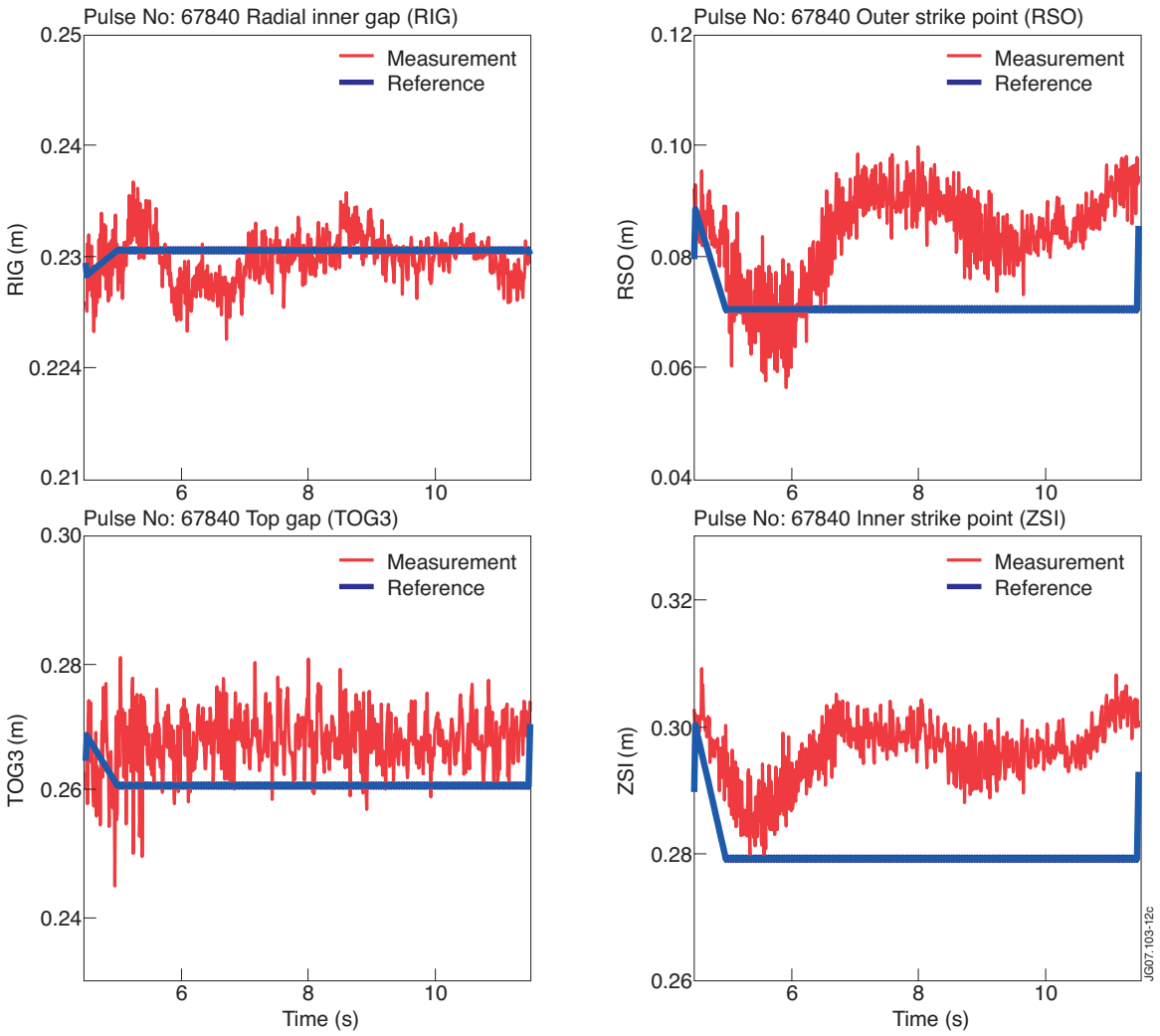

Figure 12: JET Pulse No: 67840 - shape control. The time traces during the plasma boundary flux control phase of the JET Pulse No: 67840 are shown.

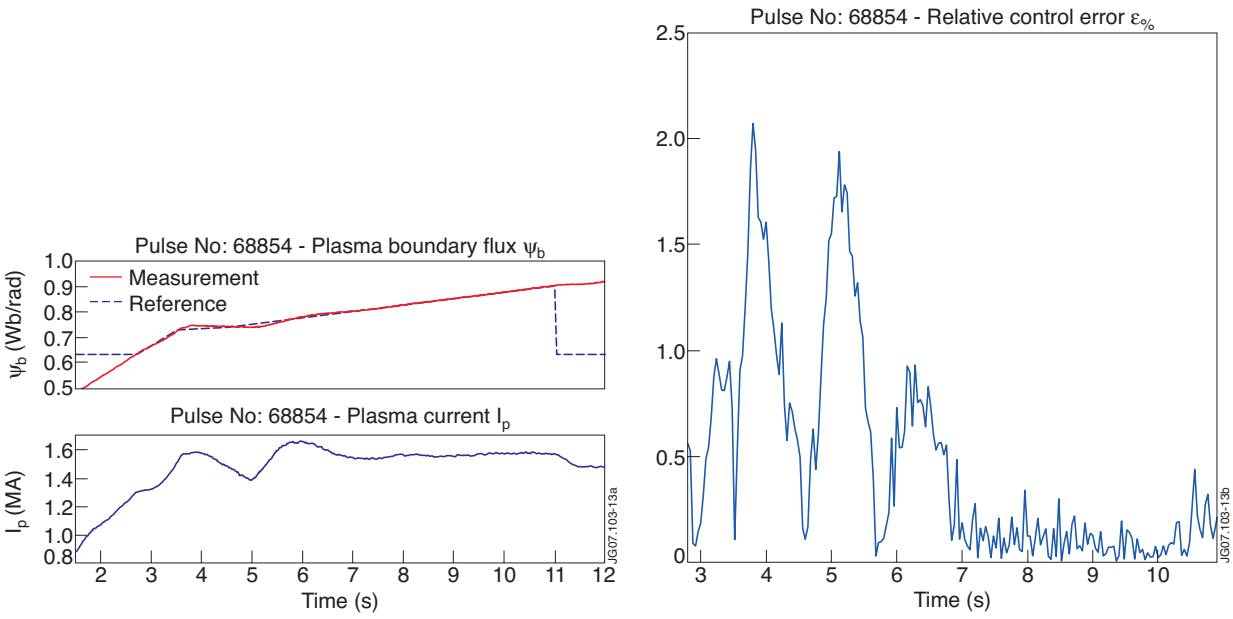

Figure 13: JET Pulse No: 68854 - boundary flux control starts at t = 2.7s during the plasma current ramp-up phase, and it stops at t = 11s.